PROCEEDINGS OF THE ROYAL SOCIETY B

Proc. R. Soc. B (2010) **277**, 2597–2605
doi:10.1098/rspb.2010.0399
Published online 14 April 2010

Calcification provides mechanical reinforcement to whale baleen α-keratin

L. J. Szewciw[1], D. G. de Kerckhove[2], G. W. Grime[3] and D. S. Fudge[1,*]

[1]*Department of Integrative Biology, and* [2]*Department of Physics, University of Guelph, 50 Stone Road East, Guelph, Ontario, Canada N1G 2W1*

[3]*Surrey Ion Beam Centre, University of Surrey, Guildford, Surrey GU2 7XH, UK*

Hard α-keratins such as hair, nail, wool and horn are stiff epidermal appendages used by mammals in a variety of functions including thermoregulation, feeding and intraspecific competition. Hard α-keratins are fibre-reinforced structures consisting of cytoskeletal elements known as 'intermediate filaments' embedded in an amorphous protein matrix. Recent research has shown that intermediate filaments are soft and extensible in living keratinocytes but become far stiffer and less extensible in keratinized cells, and this stiffening may be mediated by air-drying. Baleen, the keratinous plates used by baleen whales during filter feeding, is an unusual mammalian keratin in that it never air dries, and in some species, it represents the most heavily calcified of all the hard α-keratins. We therefore tested the hypothesis that whale baleen is stiffened by calcification. Here, we provide, to our knowledge, the first comprehensive description of baleen material properties and show that calcification contributes to overcoming the shortcomings of stiffening this hard α-keratin without the benefit of air-drying. We also demonstrate striking interspecies differences in the calcification patterns among three species of baleen whales and provide novel insights into the function and evolution of this unusual biomaterial.

Keywords: whale baleen; alpha-keratin; calcification; proton-induced X-ray emission; transmission electron microscopy; biomechanics

1. INTRODUCTION

Hard α-keratins are mammalian biomaterials that make up stiff epidermal appendages such as hair, wool, nail, hoof and horn (Fraser *et al.* 1972; Homberger 2001). At the cell and molecular levels, hard α-keratins consist of keratinocytes filled with 10 nm-wide protein filaments known as 'intermediate filaments' that are embedded in an amorphous protein matrix (Fudge & Gosline 2004). The structure and mechanical behaviour of conventional α-keratins are well described (Bendit & Feughelman 1968; Hearle 2000). Briefly, wool fibres have an initial tensile modulus (E_s) of about 2 GPa and an extensibility (or strain at fracture) (ε_b) of about 0.50, and these properties are relatively insensitive to hydration levels (Feughelman 2002). By contrast, hydrated preparations of isolated intermediate filaments or bundles *in vitro* are far softer ($E_s = 7$ MPa) (Fudge *et al.* 2003) and more extensible ($\varepsilon_b = 2.5$) (Kreplak *et al.* 2005) than wool, and these values change drastically when the fibres are dried. Specifically, E_s increases by about three orders of magnitude and ε_b drops to about 1.0 (Fudge & Gosline 2004). Based on these observations, we recently proposed that the intermediate filaments in wool are maintained in an effectively dry state even when the fibres are in a hydrating environment (Fudge & Gosline 2004). Intermediate filaments assemble within the aqueous environment of a living keratinocyte, which raises the question of how the filaments initially become dehydrated in a developing hard α-keratin. One possibility is air-drying of the filaments, accompanied by cross-linking of the keratin matrix around them.

If air-drying is the primary mechanism of stiffening in hard α-keratins like wool, then another mechanism must be at play in hard α-keratins such as whale baleen, which never has an opportunity for air-drying. Baleen makes up the filter-feeding apparatus used by baleen whales, and consists of racks of keratinous plates that are frayed along their lingual edge into a fringe of tapered bristles that acts as a sieve for filtration of prey (figure 1; Williamson 1973; Werth 2000; Fudge *et al.* 2009). Little is known about the material properties of whale baleen aside from one study on the effects of petroleum on baleen plates (St Aubin *et al.* 1984).

Baleen is the most highly calcified keratin, and while levels vary among species, some like the sei whale (*Balaenoptera borealis*) have baleen that consists of 14.5 per cent hydroxyapatite (dry weight) (Pautard 1963; 1965). Humpback (*Megaptera novaengliae*) and minke (*Balaenoptera acutorostrata*) baleen bristles have been shown to contain intermediate (up to 4%) and low (about 1%) calcium salt concentrations, respectively (Pautard 1963; St Aubin *et al.* 1984). Calcification has been proposed to increase the abrasion resistance of bristles (Pautard 1963), promote fraying of the baleen plate into bristles (Pautard 1963) and provide bristles with 'greater flexibility and strength' (Halstead 1974). Here, we tested the hypothesis that baleen calcification compensates for some of the mechanical deficiencies that arise from building a hard α-keratin without the benefits of air-drying. We tested the predictions that calcification would increase the tensile modulus and yield

* Author for correspondence (dfudge@uoguelph.ca).

Received 25 February 2010
Accepted 25 March 2010

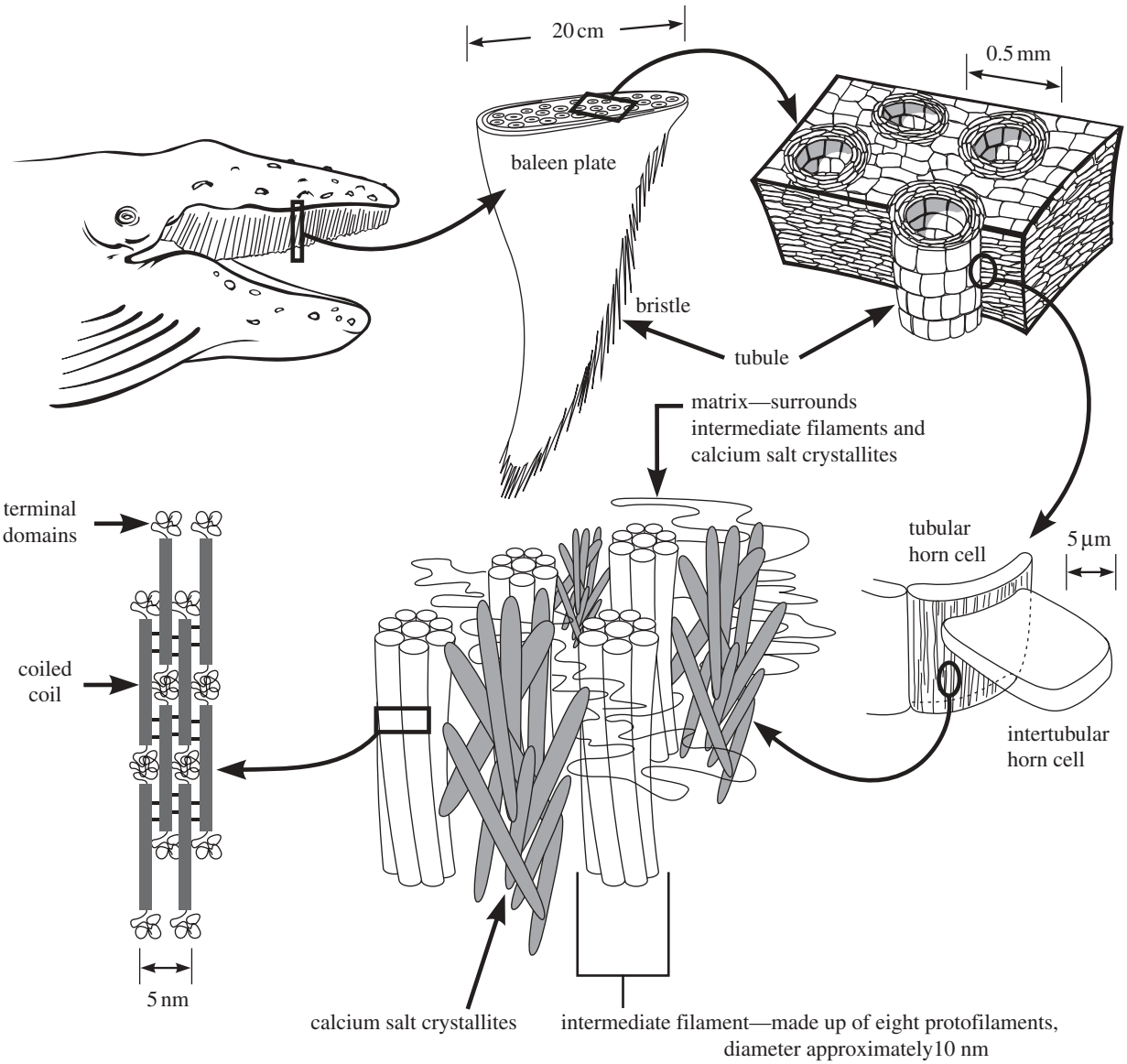

Figure 1. Hierarchical morphology of humpback whale baleen, from the level of the whole baleen apparatus down to the level of protein domains within 10 nm intermediate filaments. In the current study, mechanical tests were performed on bristles that were detached from the lingual edge of baleen plates. Baleen plates consist of horn tubules embedded in intertubular horn. Bristles are simply tubules that have become exposed at the lingual edge owing to the wearing away of intertubular horn. This diagram applies to the structure of baleen in all rorqual whales, but significant variation exists among species with regard to the amount and location of calcium salt crystallites.

stress of baleen. To better understand the role of calcium salts in baleen, we also investigated the distribution of calcium in three rorqual species using three techniques, von Kossa staining, proton-induced X-ray emission (PIXE) and transmission electron microscopy (TEM). These results demonstrate unique patterns of calcium distribution among the baleen of all three whales and suggest possible differences in function.

2. MATERIAL AND METHODS

(a) *Sample collection, preservation and preparation*

Baleen samples from five different rorqual whales (one sei, one humpback and three minke) were used for these experiments. Sei baleen came from a 14.0 m male that washed ashore dead at Baccaro Point near Shelburne, Nova Scotia, Canada. Humpback baleen came from an 11.6 m female that washed ashore dead at Phinney's Cove in Annapolis Valley, Nova Scotia, Canada. The first minke baleen sample came from a 4.75 m female that was found dead at Hopewell Cape, Albert Co., New Brunswick, Canada. The second minke baleen sample came from a 4.90 m female that was euthanized at Little Joggins Cove near Digby, Nova Scotia, Canada. The third minke baleen sample came from a 4.88 m female that was found dead at Miramichi River at Nelson Junction, New Brunswick, Canada. All baleen samples were stored in 0.5 per cent sodium azide in artificial sea water (34‰) at 4°C until use. While we do not know the hydration state of the baleen before it was placed in storage solution, we suspect that the relative humidity inside the mouth of a rotting whale is close to 100 per cent. Furthermore, the minke sample obtained from the euthanized whale never dried out and was similar to the other two in its material properties.

Baleen bristles were detached from the proximal 80 per cent of the curved length of a main baleen plate by severing them at their point of attachment to the plate. Bristle lengths were approximately 20 cm for sei and humpback and 10 cm

for minke. To test for the effects of calcification on baleen mechanics, some bristles from each sample were decalcified prior to tensile testing by 24 h of immersion in Surgipath Decalcifier II (Surgipath Canada Inc., Winnipeg, Manitoba, Canada) at a volume 20 times the volume of the wet bristles. After decalcification, bristles were rinsed with distilled water and stored in calcium-free saltwater (450 mM NaCl). For three of the five baleen samples, the efficacy of bristle decalcification was verified with atomic absorption spectroscopy (AAS) of natural and decalcified bristles. Only specimens free of kinks and nicks were used in tensile tests. Specimens always contained the proximal end of the bristle. The average specimen length for each baleen sample was about 3 cm, and length between the grips was set at 2.25 cm. Cyanoacrylate adhesive was used to glue each bristle end between two 3×3 cm Bristol board squares and a permanent marker was used to mark both ends of the exposed portion of the specimen. The position of these marks was monitored during testing to check for slippage.

(b) *Tensile tests*

Tensile tests were performed using an Instron Universal Testing Machine (UTM), Model 3343, fitted with immersible pneumatic grips and a BioPuls water bath, resting atop an anti-vibration air table. Specimens were clamped to the UTM using pneumatic grips that held the Bristol board supports. Clamping pressures were typically between 350 and 700 kPa. The upper grips were attached to the 10 N load cell of the UTM (or 100 N load cell for humpback specimens), and the lower grips to a column within the water bath. Resolution of the 10 N load cell was 0.5 mN. Specimens were immersed in sea water for 2 min before the start of the tensile test in the water bath at room temperature (approx. 20°C) to replace any water that might have been lost during the short mounting procedure in air. Control specimens were rehydrated and tested in artificial sea water (34‰), whereas decalcified specimens were rehydrated and tested in calcium-free saltwater of similar ionic strength (450 mM NaCl).

Data collection was performed using a computer running Instron Bluehill v. 2.9 software. Specimens were extended at a rate of 5 mm min^{-1} to remove slack and load and extension values were zeroed when the load reached a threshold value of 5 mN. Specimens were extended at 10 mm min^{-1} (or a strain rate of $5.6 \times 10^{-3}\ \text{s}^{-1}$) and data captured at 10 Hz. If slippage was observed or if a specimen broke at or within the grips, the data were discarded. After testing, specimens were cross sectioned with a razor blade at 50 per cent grip length and cross sections were mounted on a glass slide under a coverslip in sea water. Sections were imaged with a Nikon Eclipse 90i microscope using a Q-Imaging colour QI camera. Bristle cross-sectional area was measured from images of tubule cross sections with NIS-Elements AR 3.0 imaging software. All mean values reported are followed by the standard error of the mean ($\pm$s.e.). Mean cross-sectional areas at 50 per cent grip length for the three bristle types were $4.14 \pm 0.32 \times 10^{-2}\ \text{mm}^2$ for sei ($n = 20$), $1.40 \pm 0.09 \times 10^{-1}\ \text{mm}^2$ for humpback ($n = 32$) and $2.10 \pm 0.14 \times 10^{-2}\ \text{mm}^2$ for minke ($n = 13$). Inner tube diameters at 50 per cent grip length were $6.64 \pm 0.25 \times 10^{-2}$ mm for sei ($n = 20$), $1.42 \pm 0.07 \times 10^{-1}$ mm for humpback ($n = 32$) and $6.82 \pm 0.21 \times 10^{-2}$ mm for minke ($n = 13$). Outer tube diameters at 50 per cent grip length were $2.36 \pm 0.09 \times 10^{-1}$ mm for sei ($n = 20$), $4.42 \pm 0.13 \times 10^{-1}$ mm for humpback ($n = 32$) and $1.77 \pm 0.05 \times 10^{-1}$ mm for minke ($n = 13$).

Calculations of Young's modulus (or stretching modulus, E_s, in GPa), yield stress (MPa), yield strain, breaking stress (MPa) and breaking strain were carried out by the Bluehill software. Young's modulus was calculated from the slope of the initial linear portion of the stress–strain curve. Plateau slopes were calculated from tensile stress–strain data between strains of 0.1 and 0.3. Final slopes were calculated from tensile stress–strain data between strains of 0.38 and 0.42. Yield point was calculated as the point at which the modulus decreased to 80 per cent of its initial value. Breaking point was calculated as the location on the stress–strain curve at 99 per cent the maximum load. Whereas the inner tube diameter remained constant along the grip length, all bristles showed some degree of taper in the outer tube diameter, with the outer diameter decreasing on average at a rate of $1.99 \pm 0.19 \times 10^{-3}$ for sei ($n = 20$), $3.19 \pm 0.21 \times 10^{-3}$ for humpback ($n = 30$) and $1.75 \pm 0.17 \times 10^{-3}$ for minke ($n = 12$) along the grip length from the proximal to distal ends. To quantify potential effects of bristle taper on our estimates of material properties, we examined the relationship between the degree of specimen taper (measured as the per cent decrease in the cross-sectional area over the grip length) and E_s, yield stress and yield strain. We confined this analysis to minke bristles to avoid potentially confounding effects of calcification. Extrapolation of these data to the y-intercept allowed us to estimate the values we might have obtained in the absence of specimen taper. From this analysis, we estimate that specimen taper in minke bristles may result in 22, 30 and 12 per cent underestimations of E_s, yield stress and yield strain, respectively. These values are consistent with estimates obtained from a tapered rod computational model we constructed to calculate the direction and magnitude of taper effects on estimates of bristle mechanical properties. While these are substantial potential errors, they are not large enough to affect the main conclusions of this study.

Wool fibres were obtained from six different Dorset-Rideau sheep and stored in air until their use in tensile tests. Fibres were prepared, tested, imaged and their data analysed, in much the same way as baleen bristles. Wool fibres were tested in distilled water under the same conditions as baleen bristles. Fibres were then mounted on a microscope slide in distilled water and imaged at 50 per cent grip length. Fibre diameter was measured using Image J 1.36b software and entered into the Bluehill software for calculation of specimen cross-sectional area (assuming fibre circularity) and specimen mechanical properties. No evidence of taper was found in wool fibres.

(c) *Flexural tests*

Three-point flexural tests were performed on natural baleen bristle specimens from sei, humpback and minke sample 3 baleen. Flexural tests on decalcified specimens were commenced but terminated owing to obvious delamination of keratin layers. Specimens were tested on a custom-made three-point flexural test platform that consisted of a plastic well with two triangular notches cut into the opposing sides. The inner diameter of the well, and thus the specimen support span, was 20 mm and the wall thickness was 1.5 mm. Specimens were centred on the platform, with an overhang length of 0.5 mm on either side. The well was filled with water, but specimens never contacted the water

Table 1. Mean tensile test results for natural and decalcified (decalc.) wool fibres and sei, humpback and minke whale baleen bristles. (n = number of wool fibres or baleen bristles tested from each sample.)

	E_s (MPa)	n	yield stress (MPa)	n	yield strain	n	breaking stress (MPa)	n	breaking strain	n
wool ($N = 6$)	1216	37	24	36	0.028	36	110	37	0.50	37
decalc. wool ($N = 1$)	1269	25	24	25	0.024	25	118	19	0.50	19
sei ($N = 1$)	1188	28	11	28	0.012	27	30[a]	24	0.35[a]	23
decalc. sei ($N = 1$)	637	29	6.7	24	0.014	24	18[a]	21	0.52[a]	21
humpback ($N = 1$)	1225	31	15	31	0.015	31	36	31	0.53	31
decalc. humpback ($N = 1$)	971	50	11	44	0.013	44	33	6	0.47	6
minke ($N = 3$)	652	33	7.1	26	0.014	26	27	21	0.47	21
decalc. minke ($N = 2$)	636	37	7.2	32	0.014	32	26	17	0.49	17

[a]Samples for which failure data were highly variable owing to fraying of samples at high strains.

during tests. The entire apparatus was covered with a plastic tent during tests to minimize dehydration. Flexural tests on hydrated, dehydrated and rehydrated bristles indicated that specimen dehydration during mounting was minimal and that specimens were fully hydrated during testing. The compressor, which was attached to the load cell of the UTM, was a custom-made aluminium rod with a flat, circular face 2 mm in diameter at its tip. Load data from the 10 N load cell were collected at 10 Hz as the sample was bent at a rate of 1 mm min^{-1} to a maximum deflection of about 1 mm. Specimens were cross sectioned with a razor blade at 50 per cent specimen length and imaged in the same way as the tensile specimens. IMAGE J software was used to calculate the second moment of area (I) for each cross section, defined as $I_x = \int y^2\, dA$, where dA = an elemental area and y = the perpendicular distance from the x-axis to the element dA (Pilkey 2002). Bending modulus, E_b, of each specimen was calculated as $E_b = (F/d \cdot l^3)/(48I)$ (Vogel 1988), where F/d is the initial slope of the load–displacement curve, and l is the support span. This equation assumes that deflections owing to shear are negligible, which should be the case for the set-up we used, where the ratio of support span distance to bristle diameter was 45 or greater (Spatz *et al.* 1996). This equation also assumes that the material is homogeneous, isotropic and linearly elastic. Baleen bristles do not fulfil these criteria, but the point of the bending tests was not to determine the exact value of the bending modulus, but rather to compare values among the three baleen types.

(d) *Atomic absorption spectroscopy*

To verify the efficacy of bristle decalcification, natural and decalcified wool fibres and baleen bristles from all three species were analysed with AAS for calcium, phosphorus and sulphur. All specimens were rinsed with and stored in distilled water prior to testing. Calcium, phosphorus and sulphur concentrations were calculated as $\mu g\, g^{-1}$ dry weight of tissue.

(e) *von Kossa staining*

Samples for von Kossa staining were taken at the distal end of the baleen plate at the labial edge. Five micron-thick sections were made from paraffin-embedded blocks using a Leica RM 2155 microtome with a stainless-steel knife. Cross sections were stained for calcium salts using a von Kossa staining protocol, in which calcium reacts with silver nitrate and light to yield metallic silver. Optical micrographs were taken with a Nikon Eclipse 90i microscope using a Q-Imaging colour QI camera and NIS-ELEMENTS AR 3.0 software.

(f) *Proton-induced X-ray emission*

Baleen from all three species was analysed by PIXE (Johannson & Campbell 1988) to generate two-dimensional elemental maps of calcium, phosphorus and sulphur in baleen cross sections. Specimens were cut from a main baleen plate, dehydrated in an ethanol series (30 min in 50, 70 and 90% EtOH, and 5 h in 100% EtOH) and embedded in LR White Embedding Medium according to manufacturer's instructions. Specimens embedded in polymerized resin were cut with a bandsaw to a section width of about 1 cm. One section was turned on a lathe to create a smooth surface and polished with fine-grade Carborundum Flexbac Polishing Paper. The smooth face was cleaned with reagent grade EtOH, carbon-coated using an Edwards AUTO 306 Vacuum Coater and stored in a desiccator. Micro-PIXE, using a proton beam approximately 2 μm in diameter (beam energy 2.582 MeV, current 100 pA; Simon *et al.* 2004), was performed on all baleen specimens to generate PIXE maps for calcium, phosphorus and sulphur distributions.

Induced X-rays were detected using an 80 mm^2 Sirius Si(Li) detector with a Titan digital X-ray pulse processor (both from e2V Scientific Ltd). Elemental maps were produced by creating windows on specific X-ray peaks using the Oxford Microbeams OMDAQ software package (Grime & Dawson 1995). Elemental molar ratios were obtained by fitting the X-ray spectra using the GUPIX software package (Maxwell *et al.* 1989). A 130 μm Be filter was fitted over the Si(Li) detector window to avoid the degradation of the detector performance caused by high-energy recoiling protons entering the detector. The energy response function of the detector and filter was determined at intervals by analysing a standard reference material (lead glass type BCR-126A from IRRM, Geel, Belgium).

(g) *Transmission electron microscopy*

Tissue from the middle of a sei main baleen plate was dissected out and embedded in LR White resin. Tissue blocks were sectioned with a Reichert-Jung Ultracut E microtome fitted with a diamond knife. Sections were mounted on copper grids and imaged unstained with an LEO 912 AB TEM at magnifications between ×5000 and ×100 000.

3. RESULTS

(a) *Tensile and flexural tests*

Baleen bristles of all types exhibited an E_s that was similar to values for other hydrated hard α-keratins, and far higher than values for hydrated intermediate filament bundles (Fudge *et al.* 2003; table 1 and figure 2). Mean

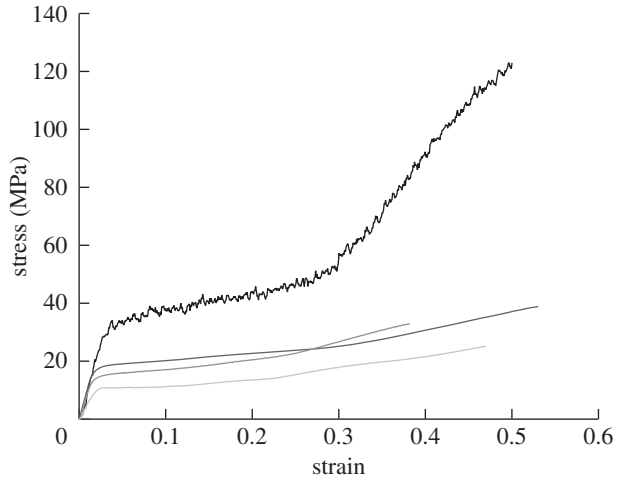

Figure 2. Representative stress–strain curves from tensile tests on wool fibres, and on sei, humpback and minke whale baleen bristles. Note how wool (upper curve) has a higher strength and yield stress than all three baleen types, but a similar initial modulus. Black line, wool; dark grey, humpback; grey, sei; light grey, minke.

E_s of baleen bristles was 0.65 ± 0.03 GPa collectively for the three minke samples, and 1.19 ± 0.05 GPa and 1.22 ± 0.06 GPa for sei and humpback bristles, respectively. The mean E_s of wool fibres from the six wool samples was 1.22 ± 0.04 GPa. As predicted, baleen bristles exhibited a lower tensile yield stress than wool fibres (table 1 and figure 2), with mean values of 7.1 ± 0.3, 11.0 ± 0.5, 15.1 ± 0.6 and 24.2 ± 0.9 MPa for minke, sei, humpback and wool, respectively. Baleen bristles exhibited a consistently lower yield strain than wool fibres (table 1 and figure 2), with a mean of 0.014 ± 0 for baleen, and 0.028 ± 0.002 for wool. Both baleen bristles and wool fibres failed at a strain of approximately 0.50, but wool fibres reached a higher stress before failure (table 1 and figure 2). Average slopes of the plateau region of tensile stress–strain curves calculated between strain values of 0.1 and 0.3 were 73.5 ± 3.5 MPa for wool, 31.3 ± 1.4 MPa for humpback and 35.7 ± 1.7 MPa for minke. Average slopes of the final region of tensile stress–strain curves calculated between strain values of 0.38 and 0.42 were 352 ± 14 MPa for wool, 42.7 ± 2.7 MPa for humpback and 53.0 ± 4.1 MPa for minke, demonstrating that strain stiffening was lower in baleen than in wool. Elastic moduli for baleen bristles tested in flexure (E_b) were lower than values measured in tension, but roughly consistent in their relative magnitude among the three species. Mean E_b values were 0.31 ± 0.02 GPa for minke, 0.71 ± 0.03 GPa for humpback and 0.72 ± 0.02 GPa for sei.

Minke, humpback and sei baleen bristles contained low, intermediate and high calcium salt concentrations, respectively (table 2). Bristles with the highest levels of calcium salts, i.e. sei bristles, had higher E_s, E_b and yield stress values than minke bristles, which were low in calcium. To test more directly the idea that calcification increases the tensile modulus and yield stress, we performed tensile tests on decalcified baleen bristles (table 1 and figure 3). Decalcification, which was confirmed using AAS (table 2), caused the greatest decrease in E_s (46%) for sei bristles, a lesser decrease in E_s (20%) for humpback bristles and had little effect on the tensile properties of minke bristles (2%). After decalcification, sei bristle E_s and yield stress decreased to 0.64 ± 0.02 GPa and 6.7 ± 0.3 MPa, respectively, similar to the E_s and yield stress of minke bristles in either calcification state. Decalcified humpback bristles had an E_s and yield stress of 0.97 ± 0.03 GPa and 10.8 ± 0.4 MPa, respectively. Decalcification had no effect on the yield strain of baleen bristles and little effect on the tensile mechanics of wool fibres, which are naturally low in calcium, causing a slight increase (4%) in E_s, no change in yield stress and a slight decrease (14%) in yield strain.

Table 2. Calcium, phosphorus and sulphur content ($\mu g\, g^{-1}$ dry weight) of natural and decalcified (decalc.) wool fibres and sei, humpback and minke whale baleen bristles measured using AAS. (All values are based on a single sample, except for the natural minke baleen values, which are an average of values from two samples.)

	calcium ($\mu g\, g^{-1}$)	phosphorus ($\mu g\, g^{-1}$)	sulphur ($\mu g\, g^{-1}$)
wool	2800	150	31 000
decalc. wool	<32	120	32 000
sei	41 000	18 000	23 000
decalc. sei	180	390	28 000
humpback	7900	2900	39 000
decalc. humpback	670	780	34 000
minke	2500	1400	27 000
decalc. minke	21	260	27 000

(b) *von Kossa staining*

Calcification patterns for all three species were examined using von Kossa stained cross sections from the distal end of the labial edge of main baleen plates (figure 4). The largest tubules in humpback and sei baleen contained concentric rings of calcium salts that increased in density from the outer to the inner tubule cortex. The largest tubules in minke baleen contained rings of calcium salts located only within the inner tubule cortex. The calcium salt rings in minke tubules often formed a single thick band, or sometimes two bands, of several calcified tubule lamellae within the inner cortex (figure 4). By contrast, calcium salt rings in humpback and sei tubules formed multiple thin rings of calcified tubule lamellae separated by intervening layers of relatively uncalcified cells (figure 4). The smallest tubules in all baleen types contained a high density of calcium salt rings and resembled the inner cortex of the largest tubules. The intertubular horn of minke baleen was calcified, whereas the intertubular horn of humpback and sei baleen was uncalcified. Sections from the two minke specimens examined showed the same calcification pattern.

(c) *Proton-induced X-ray emission*

Two-dimensional PIXE maps of calcium and phosphorus distributions in baleen cross sections were similar to the patterns revealed by von Kossa staining (figure 5). Sulphur maps were negatively correlated with calcium and phosphorus, suggesting a mutual exclusion of calcium phosphate salts and protein (figure 5). Analysis of the PIXE data revealed a molar ratio of calcium to

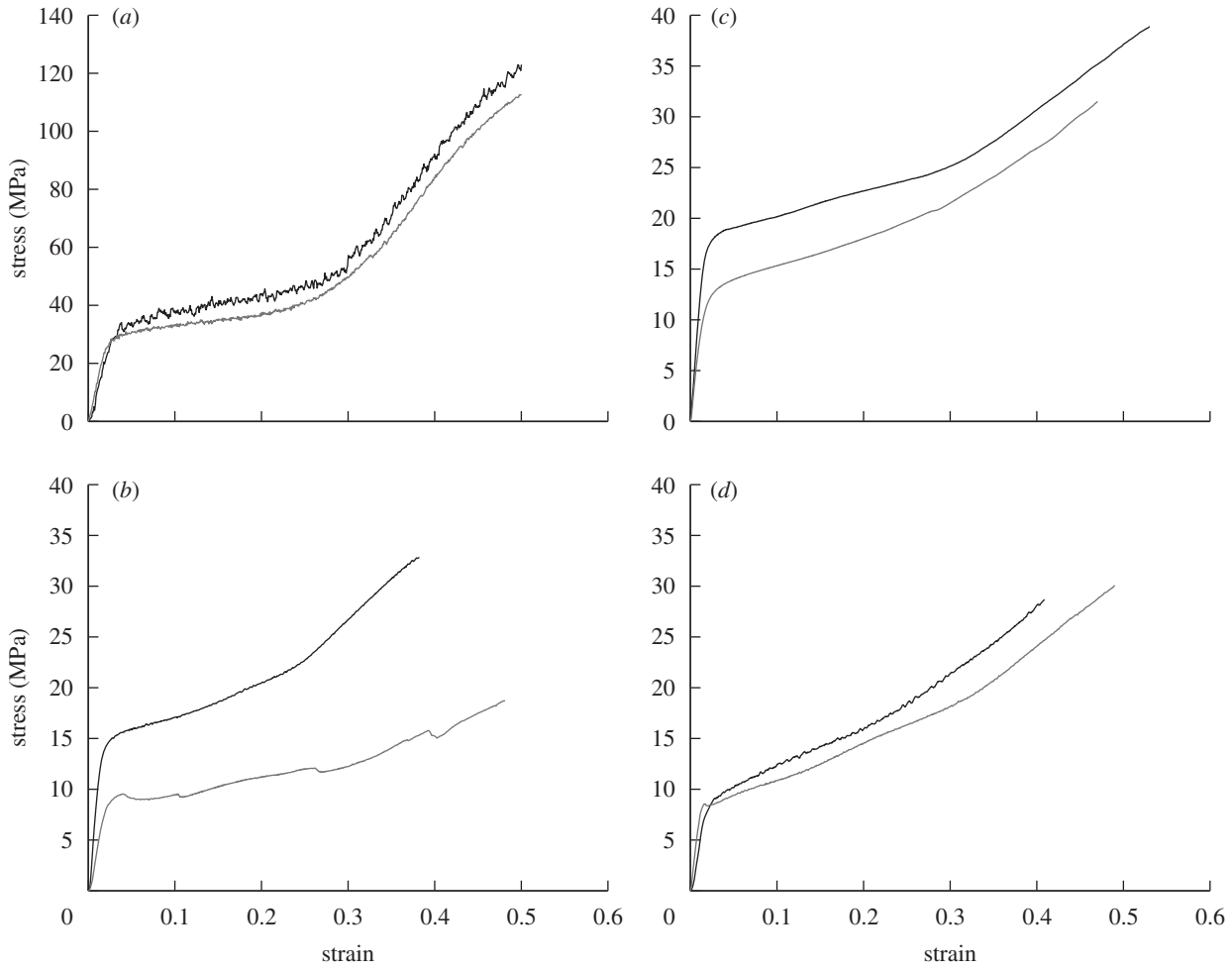

Figure 3. Representative stress–strain curves from tensile tests on (*a*) natural and decalcified wool fibres, and (*b*) natural and decalcified sei, (*c*) humpback and (*d*) minke whale baleen bristles. Note how decalcification leads to a decrease in the initial modulus and yield stress of the two most highly calcified baleen types (humpback and sei), whereas decalcification has little effect on these values for minke baleen and wool. Black lines, natural; grey lines, decalcified.

phosphorus of 1.67 ± 0.03, which is consistent with the 5 : 3 molar ratio one would expect from hydroxyapatite, which others have hypothesized is present in whale baleen (Pautard 1962, 1963; St Aubin *et al.* 1984).

(d) *Transmission electron microscopy*

TEM allowed us to resolve the calcification pattern shown using von Kossa staining and PIXE with greater detail (figure 6*a*). TEM micrographs of sei whale tubular horn confirmed the presence of rod-shaped mineral crystallites first described by Pautard (1962, 1981) (figure 6*b*). Regions of highest calcification in sei samples appeared almost fully impregnated with calcium salts, and these regions were bordered on the side facing the tubule medulla by cells that appeared almost completely devoid of calcium salts. On the side facing the tubule periphery, calcification levels decreased gradually to the minimum level over a distance of about four or five cell widths. This 'sawtooth' pattern of calcification levels was also observed in high power light micrographs of von Kossa stained sections (figure 6*c*).

4. DISCUSSION

We investigated the hypothesis that calcium salts are used to modify the material properties of baleen α-keratin in a way that partly compensates for the shortcomings of stiffening in a wet environment. This hypothesis predicts that baleen with greater calcification should exhibit a higher modulus and yield stress than less-calcified baleen, and our results were mostly consistent with this prediction. Furthermore, decalcification caused the greatest decrease in the tensile modulus and yield stress of sei baleen, the smallest decrease for minke baleen and an intermediate decrease for humpback baleen, which exhibits an intermediate level of calcification. Decalcification had no effect on the yield strain, suggesting that it is governed entirely by the mechanical behaviour of the coiled coils within intermediate filaments (Hearle 2000). It is interesting that the material properties of sei and humpback baleen are so similar given that sei baleen is considerably more calcified. This result suggests that there may be other mechanisms of stiffening at work in humpback baleen.

The PIXE results suggest that the calcium salt in all three baleen types is hydroxyapatite, the dominant calcium salt in bone (Pautard 1962). A major difference between bone and calcified keratin is that calcification in bone is an extracellular process, whereas in α-keratins, calcium salt crystals form within cells (Pautard 1981). From the AAS data, we can estimate the volume fraction of hydroxyapatite in sei baleen to be about 4.5 per cent,

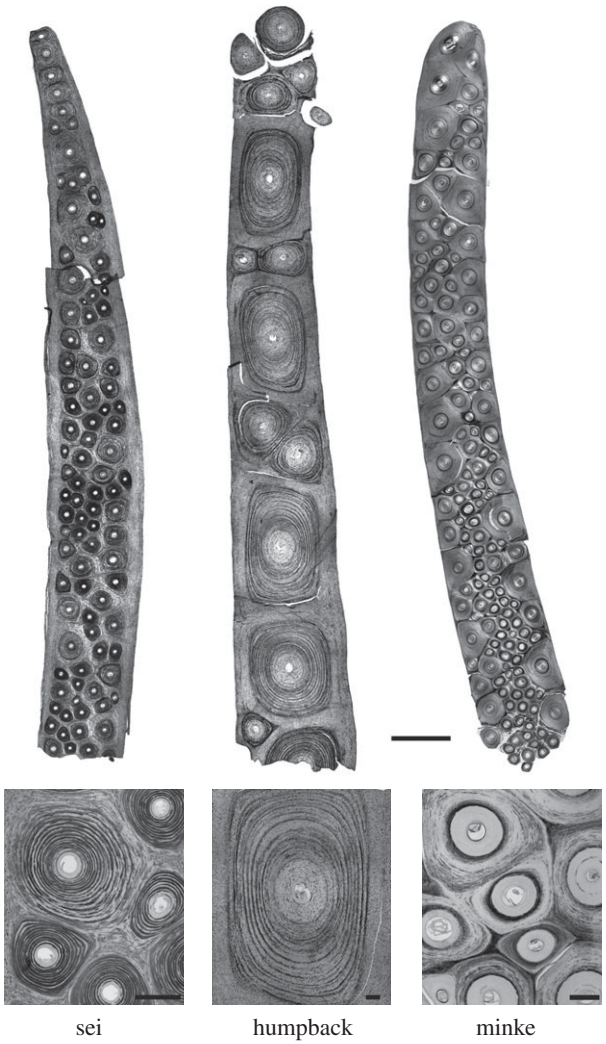

Figure 4. Transverse sections of baleen prepared using a von Kossa protocol that stains for calcium salts (black). Sections were made from the distal, labial edges of main baleen plates from all three species. Scale bar for the top three panels is 500 μm, and 100 μm for the bottom three panels.

assuming a mass fraction for calcium of 0.399, and densities of hydroxyapatite and α-keratin of 3.156 and 1.3 g cm^{-3}, respectively. Using the rule of mixtures (Wainwright *et al.* 1976), we can then calculate Young's modulus for the calcium salts in sei baleen:

$$E = E_1V_1 + E_2V_2,$$

where E is Young's modulus of the composite (1.19 GPa), and E_1V_1 refers to the product of the keratin modulus (0.637 GPa) and volume fraction (0.954), and E_2V_2 refers to the modulus of hydroxyapatite and its volume fraction (0.046). From this equation, we calculate a Young's modulus for the calcium salts in sei baleen of about 13 GPa. Published values for the modulus of hydroxyapatite are typically considerably higher (about 150 GPa for hydroxyapatite single crystals) (Saber-Samandari & Gross 2009), which suggests that one of the assumptions of the above calculation does not hold. The rule of mixtures equation assumes perfect coupling (i.e. equal strain) between the two phases, which probably does not hold, especially at higher composite strains.

While we were unable to directly measure the effects of calcification on the flexural modulus (E_b), we were able to use the natural variability in calcification among the three baleen types to explore this further. We found the ratio of E_b in highly calcified bristles (sei) to less-calcified (minke) bristles was higher than the same ratio for the tensile modulus (E_s) (2.3 versus 1.8). This suggests that calcium salts are laid down in a way that preferentially boosts E_b compared with E_s. This result is consistent with the notion that *in vivo*, bristles are more likely to be loaded in bending than in tension as a result of hydrodynamic forces, collisions with prey and abrasion from the tongue. Adaptation to flexural loading of baleen bristles is also consistent with their tubular morphology, which has greater flexural rigidity than a solid cylinder of equal cross-sectional area.

We have demonstrated that the presence of calcium salts in sei and humpback baleen increases their resistance to bending, but there is a far more straightforward way to increase flexural rigidity, and that is to increase bristle diameter. Flexural rigidity is the product of Young's modulus and the second moment of area, which is proportional to the fourth power of the radius. Large increases in flexural rigidity can therefore be effected by small increases in diameter. This raises the question of why bristle flexural rigidity is boosted via calcification rather than a simple increase in diameter. One possibility is that there are limits on how thick bristles can get before the prey-capturing function of the baleen filter is compromised. This may be particularly relevant in sei whales, which is the only rorqual species that specializes in small mesoplankton like copepods (Pivorunas 1979), and also possesses the most highly calcified baleen (Pautard 1963). In sei whales, filter porosity must be low to capture such small prey (Pivorunas 1976), and this requires fine baleen bristles. However, there is probably a limit to how fine the bristles can be before they are so floppy that they no longer form a competent filter mat between the baleen plates. In this way, calcification may have allowed for the evolution of finer bristles that were still functionally competent, which ultimately decreased filter porosity and allowed for the exploitation of smaller prey. Interestingly, bristles from right and bowhead whale baleen are known to be as fine as sei bristles (Nemoto 1959), but are relatively uncalcified (Pautard 1963; St Aubin *et al.* 1984). This may be related to the fact that these whales employ a low-speed skim-feeding behaviour that generates far lower hydrodynamic forces than more energetic lunge feeding bouts in sei whales.

If the primary function of calcification in baleen bristles is to increase their resistance to bending, one might predict that the stiffening calcium salts would be preferentially laid down at the bristle periphery, where they would have the greatest effect on the flexural rigidity. However, greater amounts of calcium salts were found near the centre of the bristles in all three baleen types (figures 4 and 5). This may be related to the fact that the baleen bristles wear over time, and if all the calcium were at the periphery, there would be a dramatic change in the flexural rigidity at the point where all of the calcium salts were completely worn away. This might create an area that is likely to kink when the bristle is loaded in bending, and would also mean that distal parts of the bristle (where the calcified regions were worn away) would not enjoy any benefits of calcification. A nested ring pattern of calcification ensures calcification of the

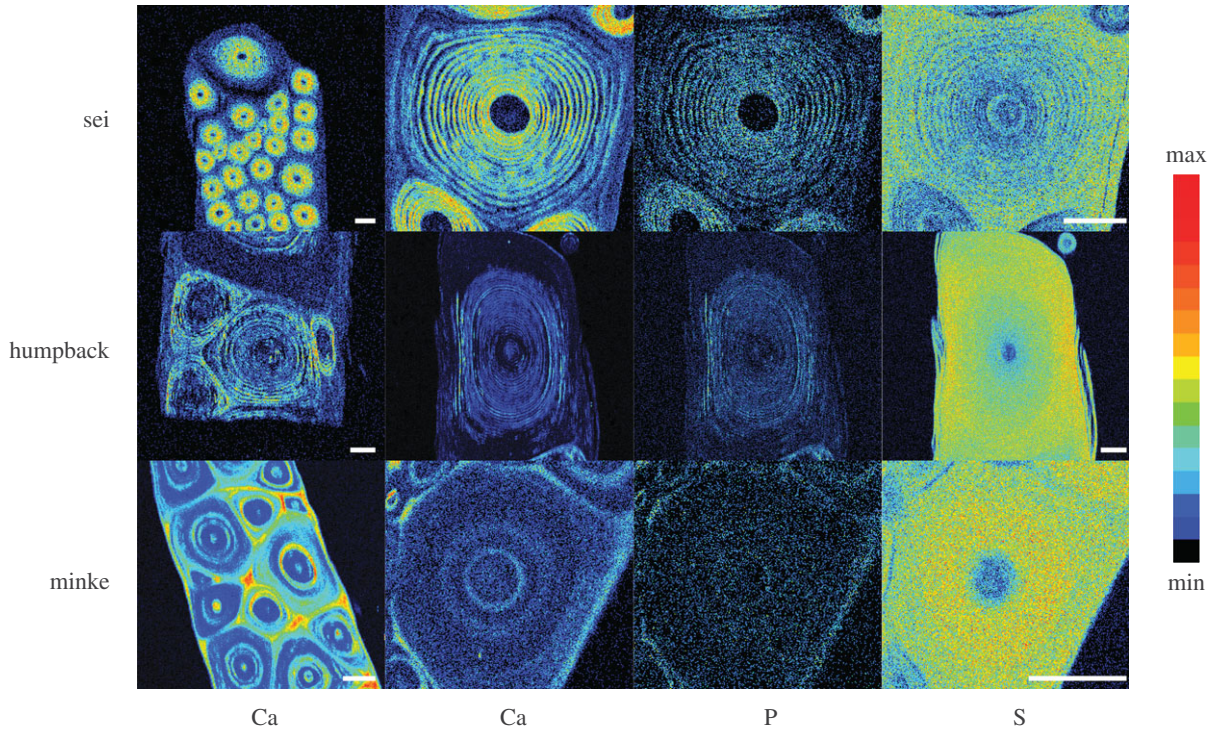

Figure 5. PIXE maps of baleen plate cross sections for calcium, phosphorus and sulphur. Within a row, the three elemental maps on the right were all generated from the same baleen tubule. Scale bars for all panels are 200 μm.

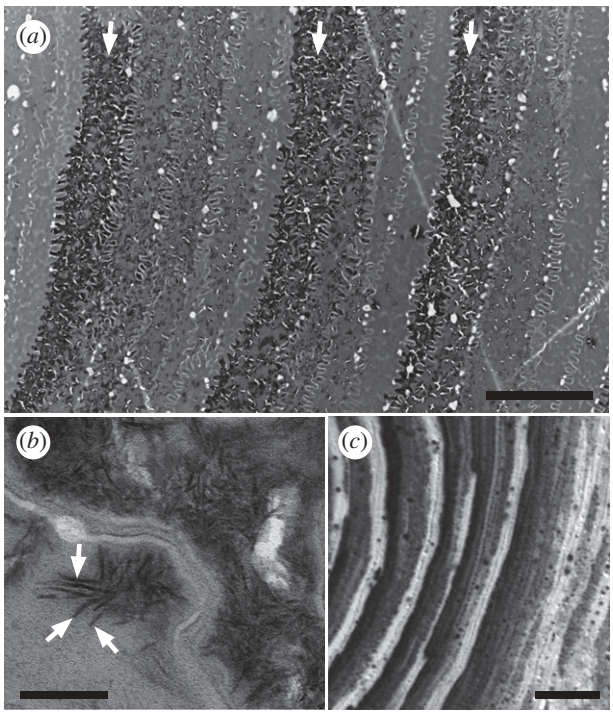

Figure 6. (*a*) TEM of a cross section of unfixed and unstained sei baleen tubular horn, showing three distinct calcium salt rings (arrows) and the pattern of gradual increase in calcium salts (dark staining regions) towards the tubule medulla (left) between calcium salt rings. (*b*) TEM micrograph of calcium salt crystallites (arrows) in sei baleen tubular horn, and (*c*) von Kossa micrograph showing the same pattern of calcification in sei baleen that is shown in (*a*). Scale bars, (*a*) 5 μm, (*b*) 100 nm and (*c*) 10 μm.

bristle along its entire length and may minimize drastic changes in flexural rigidity that could lead to kinking. Furthermore, higher calcification near the centre of a bristle may reflect a greater need for reinforcement of the finer distal portion. This notion is supported by the fact that the smallest baleen tubules we observed are typically highly calcified in a similar manner to the central portion of the largest tubules (figures 4 and 5).

Our PIXE and von Kossa data demonstrate for the first time, to our knowledge, that there are clear interspecies differences in baleen calcium salt distribution among the three rorqual species examined. The most striking difference we observed was that the intertubular horn of minke baleen is calcified, whereas in humpback and sei baleen, it is uncalcified. Minke whales specialize in larger prey items like fish and krill and therefore have little need for fine baleen bristles. It is perhaps not surprising then that minke tubular horn is relatively uncalcified, except for a few thin rings. The function of intertubular horn calcification is not clear, but we suspect that it may facilitate separation of the bristles from the intertubular horn by creating an abrupt change in material stiffness that leads to stress concentrations and cracks at the interface. In sei baleen, although the pattern is reversed, a similar mechanism could be at work, with the lack of intertubular calcification creating an abrupt interface that facilitates bristle separation.

We have clearly demonstrated that calcification of sei and humpback baleen increases the stiffness of these materials, which may be related to a lack of opportunities for air-drying. However, if one considers that decalcified and uncalcified (i.e. minke) baleen have a tensile modulus that is almost $\times 100$ higher than fully hydrated pure intermediate filaments (Fudge *et al.* 2003), this suggests that some other mechanism of stiffening is at work in baleen besides calcification. One possible mechanism is covalent cross-linking within the intermediate filaments, which could raise the modulus to something approaching that of coiled coils, or about 2 GPa (Howard 2001). Future

work should test the hypothesis that baleen is stiffened via these cross-links and investigate the nature of the keratin matrix in this unusual biomaterial.

5. CONCLUSIONS

The invasion of terrestrial habitats by amniotes was made possible in part by the evolution of α-keratins that, in conjunction with hydrophobic lipids, provided a tough, waterproof epidermal barrier. Life on land provided subsequent opportunities for stiffening α-keratins via air-drying into harder structures such as fur, nail and horn. In their re-adoption of a fully aquatic lifestyle, cetaceans forfeited the ability to stiffen α-keratins via air-drying. Here we present evidence that calcification boosts the modulus and yield stress of baleen α-keratin and therefore may compensate for the limitations of curing hard α-keratins in an aquatic environment. This mechanism may have played an important role in the tuning of bristle mechanics over evolutionary time to the demands of filter feeding in several species of baleen whales.

Special thanks to Tonya Wimmer and Donald F. McAlpine for provision of baleen samples. Wool samples were provided by Heather Bailey. Atomic absorption spectroscopy tests were performed by Nick Schrier. von Kossa stained tissue sections were prepared by David Hilchie. Specimens for TEM were prepared by Robert Harris. Thanks to Dr Chris Jeynes at the Surrey Ion Beam Centre for assistance with the PIXE experiments. Thanks also to Ian Smith for creating the line drawing. We would also like to acknowledge the contributions of three anonymous reviewers to improving our manuscript. This work was funded by the National Sciences and Engineering Research Council of Canada. Access to the Surrey Ion Beam Centre was made possible by Pump Priming funding from the Engineering and Physical Sciences Research Council of the UK.

REFERENCES

Bendit, E. G. & Feughelman, M. 1968 *Keratin. Encyclopedia of polymer science and technology*, vol. 8, pp. 1–44. New York, NY: John Wiley & Sons, Inc.

Feughelman, M. 2002 Natural protein fibers. *J. Appl. Polym. Sci.* **83**, 489–507. (doi:10.1002/app.2255)

Fraser, R. D., MacRae, T. P. & Rogers, G. E. 1972 *Keratins: their composition, structure, and biosynthesis. American Lecture Series*. Springfield, IL: Charles C. Thomas.

Fudge, D. S. & Gosline, J. M. 2004 Molecular design of the α-keratin composite: insights from a matrix-free model, hagfish slime threads. *Proc. R. Soc. Lond. B* **271**, 291–299. (doi:10.1098/rspb.2003.2591)

Fudge, D. S., Gardner, K. H., Forsyth, V. T., Riekel, C. & Gosline, J. M. 2003 The mechanical properties of hydrated intermediate filaments: insights from hagfish slime threads. *Biophys. J.* **85**, 2015–2027. (doi:10.1016/S0006-3495(03)74629-3)

Fudge, D. S., Szewciw, L. J. & Schwalb, A. N. 2009 Morphology and development of blue whale baleen: an annotated translation of Tycho Tullberg's classic 1883 paper. *Aq. Mamm.* **35**, 226–252. (doi:10.1578/AM.35.2.2009.226)

Grime, G. W. & Dawson, M. 1995 Recent developments in data acquisition and processing on the Oxford scanning proton microprobe. *Nucl. Instr. Meth. Phys. Res. B* **104**, 107–113. (doi:10.1016/0168-583X(95)00401-7)

Halstead, L. B. 1974 *Vertebrate hard tissues*. London, UK: Wykeham Publications.

Hearle, J. W. S. 2000 A critical review of the structural mechanics of wool and hair fibres. *Int. J. Biol. Macromol.* **27**, 123–138. (doi:10.1016/S0141-8130(00)00116-1)

Homberger, D. G. 2001 The case of the cockatoo bill, horse hoof, rhinoceros horn, whale baleen, and turkey beard: the integument as a model system to explore the concepts of homology and non-homology. In *Vertebrate functional morphology: horizon of research in the 21st century* (eds H. M. Dutta & J. S. Datta Munshi), pp. 317–343. Enfield, NH: Science Publishers.

Howard, J. 2001 *Mechanics of motor proteins and the cytoskeleton*. Sunderland, MA: Sinauer Associates.

Johannson, S. A. E. & Campbell, J. L. 1988 *PIXE: a novel technique for elemental analysis*. Chichester, UK: Wiley.

Kreplak, L., Bar, H., Leterrier, J. F., Herrmann, H. & Aebi, U. 2005 Exploring the mechanical behavior of single intermediate filaments. *J. Mol. Biol.* **354**, 569–577. (doi:10.1016/j.jmb.2005.09.092)

Maxwell, J. A., Campbell, J. L. & Teesdale, W. J. 1989 The Guelph PIXE software package. *Nucl. Instr. Meth. Phys. Res. B* **43**, 218–230. (doi:10.1016/0168-583X(89)90042-6)

Nemoto, T. 1959 Food of baleen whales with reference to whale movements. *Sci. Rep. Whales Res. Inst.* **14**, 149–290.

Pautard, F. G. E. 1962 The molecular-biologic background to the evolution of bone. *Clin. Orthop.* **24**, 230–244.

Pautard, F. G. E. 1963 Mineralization of keratin and its comparison with the enamel matrix. *Nature* (*Lond.*) **199**, 531–535. (doi:10.1038/199531a0)

Pautard, F. G. E. 1965 Calcification of baleen. In *Calcified tissues, Proc. Second Europ. Symp. calcified tissues* (eds L. J. Richella & M. J. Dallemagne), pp. 347–357.

Pautard, F. G. E. 1981 Calcium phosphate microspheres in biology. *Prog. Cryst. Growth Character. Mater.* **4**, 89–98.

Pilkey, W. D. 2002 *Analysis and design of elastic beams*. New York, NY: John Wiley & Sons, Inc.

Pivorunas, A. 1976 A mathematical consideration of the function of baleen plates and their fringes. *Sci. Rep. Whales Res. Inst.* **28**, 37–55.

Pivorunas, A. 1979 The feeding mechanisms of baleen whales. *Am. Sci.* **67**, 432–440.

Saber-Samandari, S. & Gross, K. A. 2009 Micromechanical properties of single crystal hydroxyapatite by nanoindentation. *Acta Biomater.* **5**, 2206–2212. (doi:10.1016/j.actbio.2009.02.009)

Simon, A. *et al.* 2004 The new Surrey ion beam analysis facility. *Nucl. Instr. Meth. Phys. Res. B* **219–220**, 405–409. (doi:10.1016/j.nimb.2004.01.091)

Spatz, H.-C. H., O'Leary, E. J. & Vincent, J. F. V. 1996 Young's moduli and shear moduli in cortical bone. *Proc. R. Soc. Lond. B* **263**, 287–294. (doi:10.1098/rspb.1996.0044)

St Aubin, D. J., Stinson, R. H. & Geraci, J. R. 1984 Aspects of the structure and composition of baleen, and some effects of exposure to petroleum hydrocarbons. *Can. J. Zool.* **62**, 193–198.

Vogel, S. 1988 *Life's devices: the physical world of animals and plants*. Princeton, NJ: Princeton University Press.

Wainwright, S. A., Biggs, W. D., Currey, J. D. & Gosline, J. M. 1976 *Mechanical design in organisms*. London, UK: Edward Arnold Publishers Ltd.

Werth, A. J. 2000 Feeding in marine mammals. In *Feeding, form, function, and evolution in tetrapod vertebrates* (ed. K. Schwenk), pp. 487–526. San Diego, CA: Academic Press.

Williamson, G. R. 1973 Counting and measuring baleen and grooves of whales. *Sci. Rep. Whales Res. Inst.* **25**, 279–292.